# Estimation of Converted Waves Static Corrections Using CMP Cross- Correlation of Surface Waves

Roohollah Askari, Robert J. Ferguson, J. Helen Isaac CREWES, Department of Geoscience, University of Calgary

## ABSTRACT

We enlarge upon the idea of CMP Cross-Correlation of Surface Waves (CCSW) to obtain an S-wave velocity model for the calculation of PS receiver static corrections. In our approach, we cross-correlate each trace of a shot record with a reference trace that is selected from within the shot gather based on high signal to noise ratio. New midpoints that relate to the correlated traces are then calculated. We calculate the phase velocity for each CMP gather, and we convert the resulting dispersion curve to an S-wave model. Our approach is faster than the conventional CCSW because in the conventional CCSW all traces within a CMP gather are cross-correlated with each other. In this study we show that, in order to have a precise estimation of a dispersion curve, we only consider those traces that lie in a spatial window and we found that the optimum window length (aperture) should be close to (one to one and half times) the maximum wavelength in a CMP gather. When the aperture is optimum, we see a high resolution image of each mode within the dispersion curve that avoids modal interferences. We obtain 2D near surface S-wave velocity models for two real data sets. By decimating traces from the first dataset, we show that we can obtain a good trend of S-wave statics relatively similar to those obtained from the original dense array data. This demonstrates that CCSW has a capacity to address static correction of converted waves when geophone spacing is wide. Using the second data set, we show the importance of wavelength-dependent aperture for estimating the phase velocity. We obtain static corrections based on an S-wave velocity model obtained from CCWS and successfully apply them to the data.

## INTRODUCTION

Converted wave data, which can provide more details about reservoirs, has been widely considered by industry in recent years. However, there are still many challenges that must be addressed. One of these is the S-wave receiver statics, which can be two to ten times greater than the P-wave receiver statics (Tatham and McCormack, 1991) due to the large $V_p/V_s$ ratio in the near surface.

We can divide S-wave receiver static correction methods into two categories. One category is data-based methods, including the CRP stack-power optimization method (Cary and Eaton, 1993) and Monte-Carlo simulated annealing (Eaton et al. 1991). The CRP stack-power optimization method gives good results where geological structures are not complex, whereas Monte-Carlo simulated annealing gives a fairly good solution but is computationally expensive (Li et al., 2012).

Another category is based on modeling the shear wave velocity. These methods are based on either refracted waves analysis (Frasier and Winterstein, 1990) or surface wave analysis (Park et al., 1999a). Although refracted waves analysis is a conventional method for the estimation of P-wave statics where a near surface velocity model is estimated, the

method is ambiguous for S-wave statics because S-wave refractions are hard to pick. Surface wave analysis is based on the inversion of the dispersion curve of ground roll, where the phase velocity as a function of frequency is inverted to an S-wave velocity model. The availability of ground roll as a predominant event in seismic data is utilized for the S-wave velocity estimation of the near surface.

Spectral Analysis of Surface Waves (SASW) (Nazarian et al., 1983) is a method to estimate S-wave velocity for the near surface. The method is based on the inversion of the fundamental mode phase velocity of ground roll. There are pairs of shots and geophones. The geophone interval is determined with regard to the frequency range of ground roll. For higher frequency components, narrower geophone spacing is designated whereas for lower frequency components, wider geophone spacing is employed. In order to have an improved signal to noise ratio, for any geophone spacing, there are two shots which are configured and reconfigured with respect to the midpoint of the geophones. Since the phase velocity and consequently the S-wave velocity are estimated with respect to a midpoint, the method provides good lateral resolution. However, the method suffers from a low signal to noise ratio (because there are only two shots and receivers), and the effect of higher modes and other types of waves (P-waves for example).

Multi-channel Analysis of Surface Waves (MASW) (Park et al., 1999a) is another method based on the analysis of dispersed ground roll. There is a shot and an array of geophones where the phase velocity of the ground roll is determined by transforming (e.g. by the phase shift method (Park et al., 1998)) the data from the time-offset domain to the frequency-slowness (or velocity) domain. The estimated phase velocity and consequently the S-wave velocity are assigned to the point in the middle of the array. Generally speaking, a MASW survey is faster than an SASW survey in the terms of data acquisition and processing. MASW also provides a better signal to noise ratio and is less affected by ambient noise since several geophones are utilized in the processing (Hayashi and Suzuki, 2004). Therefore, MASW results in better dispersion curve estimates, but at the cost of lateral resolution because the phase velocity and the S-wave velocity are not determined with respect to a midpoint between shots and receivers (Hayashi and Suzuki, 2004). In order to improve the lateral resolution in a MASW survey, smaller arrays should be used, but this reduces the resolution of the dispersion curve (Park et al., 1999b). Therefore, there is a trade-off between the estimation of the dispersion curve and lateral resolution in MASW surveys. In practice, it is critical to compensate for this trade-off. Especially in converted wave surveys, rapid spatial velocity variations in the weathering layer need to be resolved in order to compute an appropriate velocity model for static corrections. This requires both excellent quality phase velocity information as well as high spatial resolution.

In this study, we have enlarged upon the idea of CMP Cross-Correlation of Surface Waves (CCSW Hayashi and Suzuki, 2004) to increase lateral resolution. In the Hayashi and Suzuki's methodology, all traces within a common mid-point (CMP) are correlated with each other, traces with the same offset which belong the same CMP are stacked, and a dispersion curve is computed. Though this method provides good lateral resolution and a dispersion curve simultaneously, the process is computationally expensive. Therefore in our approach, to reduce cost, we cross-correlate each trace of a shot record with a

reference trace selected from within the shot gather based on high signal to noise ratio. This step removes the initial phase of a source. New midpoints that relate to the correlated traces are then calculated. We calculate the phase velocity for each CMP gather, and finally the dispersion curve is converted to a vertical shear wave velocity by an inverse procedure. By putting together all the vertical shear wave velocity profiles of all the CMP gathers, a 2D image of shear wave velocity is obtained for the data set. Since in our approach only a reference trace is cross-correlated with other trace within a CMP gather, it is faster than the conventional CCSW where all traces within a CMP gather are cross-correlated with each other, which is computationally expensive.

In this study we use two data sets. The first data set was acquired by CREWES (Consortium for Research in Elastic Wave Exploration Seismology, University of Calgary) from a site near Priddis, Alberta, Canada, about 30 km southwest of the city of Calgary. The site of the survey is located at the eastern edge of the Rocky Mountain foothills. We show that in order to have a precise estimation of dispersion curve, the maximum relative offset, which we call the aperture length in this study, must be close to (one and one and half times) the maximum wavelength of ground roll. If the aperture is too short, we see a blurred image of dispersion curves, which causes modal interference. When the aperture is optimum, we see a high resolution image of dispersion curves that avoids modal interferences. Therefore, not only does an appropriate aperture length improve dispersion curve estimation, but it also avoids the modal interference that can be so disastrous in surface waves studies (Strobbia et al., 2011). By decimating the data, we show that we can obtain a good trend of S statics similar to those obtained from the original data. This demonstrates that CCSW has a capacity to address static correction of converted waves when geophone spacing is wide. The second dataset was acquired in September 2011 by CREWES, near Hussar, Alberta, Canada. We show the importance of wavelength dependent aperture for estimating the phase velocity where there are wide ranges of wavelengths. We obtain static corrections based on an S-wave velocity model obtained from CCWS and successfully apply them to the data. We compare our static corrections result with another static corrections result obtained from PP refraction analysis scaled by 2.5 (assuming Vp/Vs ratio to be 2.5 for the near surface), and we find significant improvement of reflector coherence in the shot domain. Using our method, subsequent NMO velocity analysis shows that we obtain a better estimation of NMO velocity after applying calculated static corrections to the data.

## THEORY

If we assume that a geometrical spreading correction has been applied to surface wave data, and that $h_1(\tau)$ is the recorded signal at station 1, then the spectrum $H_2(f)$ of the signal $h_2(\tau)$ recorded at station 2 can be expressed in terms of the spectrum $H_1(f)$ of $h_1(\tau)$ as (Askari and Ferguson, 2012)

$$H_2(f) = e^{-\lambda(f)\Delta x_{1,2}} e^{-j2\pi k(f)\Delta x_{1,2}} H_1(f), \qquad (1)$$

where $H_1$ and $H_2$ are computed using the Fourier transform, $\lambda(f)$ is an attenuation function, $k(f)$ is a spatial wavenumber that characterizes the horizontal propagation of the surface wave, and $\Delta x_{1,2}=x_2-x_1$ is the distance between the two stations. For station 3 we can write its Fourier spectrum ($H_3$) in terms of the Fourier spectrum of station 1 ($H_1$).

Therefore for any specific frequency, the spatial wavenumber between $h_3$ and $h_2$ can be obtained by

$$k(f) = -\frac{\varphi_3(f)-\varphi_2(f)}{2\pi\Delta x_{2,3}} = -\frac{\Delta\varphi(f)}{2\pi\Delta x_{2,3}}, \quad (2)$$

where $\varphi_2$ and $\varphi_3$ are the absolute phase spectra of stations 2 and 3 respectively and $\Delta x_{2,3}=x_3-x_2$ is the distance between the two stations.

If we cross-correlate $h_1$ with $h_2$, the result is expressed in the Fourier domain as

$$C(H_1(f), H_2(f)) = e^{-\lambda(f)\Delta x_{1,2}} e^{-j2\pi k(f)\Delta x_{1,2}} H_1(f) H_1^*(f), \quad (3)$$

where $H_1^*$ is the complex conjugate of $H_1$. Similarly, we can write the Fourier spectra of the cross-correlated traces of $h_1$ and $h_3$ in the terms of the Fourier spectrum of $h_1$ ($H_1$) and the relative distance between $h_1$ and $h_3$ ($x_{1,3}=x_3-x_1$). With respect to the Fourier spectra of the cross-correlated traces, the spatial wavenumber between stations 2 and 3 can be also estimated by

$$k(f) = -\frac{\emptyset_3(f)-\emptyset_2(f)}{2\pi\Delta x_{2,3}} = -\frac{\Delta\emptyset(f)}{2\pi\Delta x_{2,3}}, \quad (4)$$

where $\emptyset_2$ and $\emptyset_3$ are the absolute phase spectra of the cross-correlated traces of stations 1 and 2 and stations 1 and 3 respectively. Following calculation of the wavenumber $k$, the phase velocity is obtained as

$$c_f = \frac{f}{k(f)}. \quad (5)$$

We use the approach expressed in equation 3 for the calculation of the phase velocity. Since the source effect (initial phase value) is removed, the data can be sorted into CMP gathers. Consequently, we calculate the phase velocity of traces in one CMP combined from different shots to localize our analysis spatially. In this study we use the phase shift method (Park et al. 1998) for the calculation of the phase velocity. The method is based on the estimation of the phase differences (shifts) of different traces for a range of frequencies and is able to estimate the phase velocity of multi-modal ground-roll (Askari et al., 2011).

## CMP CROSS-CORRELATION OF SURFACE WAVES

Hayashi and Suzuki (2004) introduce the idea of CMP Cross-Correlation of Surface Waves (CCSW) to increase lateral resolution. They correlate all traces within a common mid-point (CMP) with each other, traces with the same offset which belong the same CMP are stacked, and a dispersion curve is computed. Figure 1 shows the procedure used in CCSW. This approach improves the lateral resolution while keeping a good resolution of dispersion curve imaging. Since a dispersion curve is measured with respect to a fixed mid-point, the method is similar to SASW, which gives good lateral resolution. The dispersion curve is estimated by transforming multi-channel cross-correlated traces into the frequency-slowness (velocity) domain, which is similar to the idea presented in a MASW survey. Therefore the method takes the advantages of the two conventional

methods for surface wave analysis. Though this method provides good lateral resolution and a dispersion curve simultaneously, the process is computationally expensive. Therefore in our approach, to reduce cost, we cross-correlate each trace of a shot record with a reference trace selected from within the shot gather based on high signal to noise ratio. This step removes the source effect. New midpoints that relate to the correlated traces are then calculated. We calculate the phase velocity for each CMP gather, and finally the dispersion curve is converted to a vertical shear wave velocity by an inverse procedure. By putting together all the vertical shear wave velocity profiles of all the CMP gathers, a 2D image of shear wave velocity is obtained for the data set.

## FIELD DATA

We have used two converted-wave data sets in this study. The first data were acquired from a site near Priddis, Alberta, Canada, about 30 km southwest of the city of Calgary. The site of the survey is located at the eastern edge of the Rocky Mountain foothills. The 3C geophones are spaced at 2 m and the time sample interval is 1 ms. Vibroseis sources are spaced at 4 m, with a linear sweep from 10 Hz to 120 Hz, and a listening time of 10 s. Using this data set we explain the concept of aperture length, which plays an important role in successfully imaging disperse curves for the estimation of the phase velocity. The dense geophone array in the Priddis data allows us to investigate effect of geophone interval on the shear wave velocity estimation and PS statics. By decimating the data we show how shear wave velocity and PS statics are affected by changing geophone interval.

The second data set was acquired in September 2011 by CREWES near Hussar, Alberta, Canada. The survey was originally designed to test the use of different sources and receivers to investigate the extension of the seismic bandwidth into the low frequency range (Margrave et al. 2011). 10 Hz geophones were spaced at 10 m intervals along the line. A vibroseis source with a linear sweep from 1 Hz to 100 Hz, and listening time of 10 s was used. We show the importance of wavelength dependent aperture length for estimating the phase velocity for this data set. We successfully apply the calculated statics to the PS data.

## APERTURE LENGTH (PRIDDIS DATA)

We select the reference trace for each shot gather at an offset of 30 m, where the signal to noise ratio is high and wave propagation is planar (avoiding near offset effect) (Xia et al, 1999). The data are binned using a CMP bin size of 5 m to increase fold to allow for a more stable phase velocity analysis. Figure 1 shows traces in a bin where the maximum relative offset is 69 m. Figure 2 shows the phase velocity that is calculated for the data in Figure 1. The maximum observed wavelength in this record is 40 m. There are three distinct patches of dispersion curves, which are indicated by letters ‘a’, ‘b’ and ‘c’. The first approach for the estimation of a phase velocity is to choose patches ‘a’ and ‘b’ as parts of the main patch of the dispersion curve because of their good apparent coherency. Applying this approach, we will pick the solid line in Figure 2 as the fundamental mode of the dispersion curve and consider patch ‘c’ as an artifact. An alternative approach is to choose patches ‘a’ and ‘c’ as parts of the main patch of the dispersion curve. In this case, the dashed line in Figure 2 is the fundamental mode of the dispersion curve and patch ‘b’ is considered as the first higher mode of ground roll. Though the second approach seems to be more realistic, the apparent incoherency of

patches ‘a’ and ‘c’ might make us hesitant to choose it. In order to evaluate both approaches, we shorten the maximum relative offset to 45 m, which is close to the maximum length of the observed wavelength in the data (40 m) and calculate the dispersion curve. Figure 3 shows the phase velocity. Here we see two distinct patches ‘a’ and ‘b’, where patch ‘a’ is the dispersion curve (the solid line) pertinent to the fundamental mode with a tangible coherency and patch ‘b’ is the dispersion curve (the dashed line) related to the first higher mode. It can be concluded from Figure 3 that choosing the optimum length of the window for trace selection plays an important role in CCSW analysis. We call the window length ‘*aperture length*’ in this paper. It facilitates the estimation of the dispersion curves (the fundamental mode and higher modes) while maintaining good lateral resolution.

Figure 4 shows how dispersion curves evolve with respect to the aperture length. The aperture length increases from 4 m to 70 m in steps of 6 m. In the beginning, where the aperture is smaller than 20 m, a single crooked dispersion curve is observable (Figures 4a-c). Because the aperture length is not long enough with respect to the wavelength ranges, two modes (the fundamental and first higher) are superimposed. When the aperture length increases from 22 m to 34 m, we observe better trends of two modes (Figures 4d-f). This shows that dispersion curve image resolution improves with aperture increment. A good distinct image of two dispersion curves is observable in Figure 4g, where the aperture length is 40 m. Here the aperture length is equal to the maximum wavelength. High resolution images of dispersion curve are observed in Figures 4h-j, where the aperture lengths are 46 m, 52 m and 58 m. Dispersion curve resolution of the fundamental mode decreases when the aperture length increases from 64 m to 70 m (Figures 4k-l). This can be explained by near surface lateral heterogeneity. When the aperture length is long with respect to the maximum wavelength, the near surface lateral heterogeneity causes wide ranges of phase velocity for each mode at each frequency. Therefore, dispersion curve coherency becomes weak. Based on our empirical observations obtained from the analyses of different CMP gathers of the data set, an optimum aperture length is given by

$$\Gamma = \zeta \Lambda, \tag{6}$$

where $\Lambda$ is the maximum wavelength and

$$1 \leq \zeta \leq 1.5.$$

The maximum wavelength ‘$\Lambda$’ is determined by

$$\Lambda = \frac{c_{f_{max}}}{f}, \tag{7}$$

where $c_{f_{max}}$ is the maximum phase velocity of the fundamental mode. Our finding is in good agreement with a study by Ikeda et al. (2013), who propose the same criteria for an appropriate aperture length by analyzing synthetic and real data.

## S-WAVE VELOCITY MODEL FOR THE PRIDDIS DATA

We estimate the fundamental mode phase velocity for all the CDP bins in the line (Figure 5). We invert the phase velocity to a shear wave velocity model by applying inversion. We can forward model dispersion curves for any geological 1D model using Knopoff's method (Schwab and Knopoff, 1972). The Rayleigh-wave phase velocity, $c_f$, is determined by a nonlinear equation '*F*' in an implicit form:

$$F\left(f, c_f, V_s, V_p, \rho, h\right) = 0, \tag{8}$$

where $f$ is the frequency, $V_s$ and $V_p$ denote the S- and P-wave velocities, respectively, $h$ is the thickness of each layer, $\rho$ is the densities of each layers and, $c_f$ is the calculated phase velocity. Based on equation 8, it is possible to estimate an S-wave velocity model from the phase velocity through inversion. If we divide the subsurface into thin layers with constant thicknesses but with varying shear wave velocities, we can formulate equation 8 as a function of P-wave velocity, S-wave velocity and density. This approach is similar to the familiar approach used in tomography, where the subsurface is divided into small grids. In order to examine the sensitivity of the phase velocity to the shear wave velocity, P-wave velocity and density, we calculate the dispersion function's derivatives for a geological model composed of four layers (Table 1). We increase the S-wave velocity, P-wave velocity and the density of each layer by about 20% to calculate the derivatives. Figure 6 shows the calculated derivatives for the S-wave velocity, P-wave velocity, and density respectively. The phase velocity is most sensitive to the variation of the S-wave velocity. Therefore in practice, we can assign reasonable constant values of P-wave velocity, obtained from other methods (refraction methods for example), and density (Xia et al., 1999) for our inverse procedure (Figure 7) to obtain a shear wave velocity model from the phase velocity. It can be implied from Figure 6 that the frequency sensitivity ranges of the phase velocity vary with respect to the depth of the layers. For instance, the frequency sensitivity ranges for the first layer vary from 10 Hz to 50 Hz, whereas the frequency sensitivity ranges for the fourth layer vary from 1 Hz to 10 Hz. Therefore, we need lower frequency components of ground roll for the S-wave velocity estimation of the deeper layers.

The initial model is calculated from the phase velocity using the formula derived in Xia et al. (1999).

$$V_s(z) = 1.09c_f, \tag{9}$$

where $c_f$ denotes the phase velocity, $V_s$ denotes the S-wave velocity, $f$ denotes frequency, and $z$ denotes depth which is determined by

$$z = 0.5[\tfrac{v_f}{f}]. \tag{10}$$

Since the average of the wavelengths is about 40m, the maximum depth of investigation is assumed to be about 20m (the half of the maximum wavelength (Xia et al., 1999)). Figure 8 shows the predicted phase velocity (the dashed line) versus the observed phase velocity of the fundamental mode in Figure 3 (the solid line) obtained

from nine iterations using the Conjugate Gradient method. Figure 9 shows the S velocity model obtained from the phase velocity in Figure 5. Some geological features at the depths 7.5 m and 15 m are noticeable. A low velocity zone in the middle of the line (the distance from 250 m to 325 m) is detectable and is surrounded by two high velocity zones. The velocity in the right side of the low velocity zone is higher than the left side. This detailed S-wave velocity model and geological features demonstrate the potential of CCSW for near surface shear wave velocity imaging. Figure 10 (solid line) shows the static corrections calculated from the S velocity model in Figure 9. The static corrections in Figure 10 are calculated from the difference between static corrections at any CMP location and the average of the total static corrections. The detailed static corrections show the high potential usage of the method for the static correction calculation of converted waves in multi-component studies. A dramatic change of the calculated static corrections is observed around 175 m. The magnitude of the static corrections is about 20 ms, which seems to be reasonable for the first 20 m of the near surface. The reason that we are not able to image deeper layers in this study is frequency bandwidth limitation. The minimum frequency that we can observe in this data set is 11 Hz. This confines the depth of study. In practice, it is possible to increase the depth of study by using a low frequency source.

## GEOPHONE SPACING INTERVAL

In order to investigate the role of spacing interval in the calculation of static corrections, we decimate the data to have 8 m geophone spacing instead of 2 m geophone spacing, which is closer to the spacing interval in the real world. The decimated data are binned using a CMP bin size of 15 m to increase fold. The inversion parameters and procedure are the same as used for the original data. Figure 11 shows the S-wave velocity model for the decimated data. The general S-wave velocity image of the decimated data is in a good agreement with the original data (Figure 9). However, some detailed velocity variations are missing in the decimated data. For instance, the decimated model proposes a lower S-wave velocity from 80 m to 140 m distance and also exhibits a smoother lateral velocity variation from 325 m to 400 m distance. This can be explained by the sampling interval effect. When we have a finer geophone spacing, we obtain a more detailed structure of the subsurface while a wider geophone spacing provides a general image of the subsurface.

Based on the S velocity model in Figure 11, we calculate the PS statics, which are indicated by the black dashed line in Figure 10. Generally, the decimated data provides slightly smaller calculated statics compared to the original data. The calculated statics for the distance from 330 m to 420 m (the blue box in Figure 10) are larger than those for the original data because there is a high velocity abnormality surrounded by a low velocity field at these geophone locations. When geophone sampling is wider, this high velocity abnormality cannot be detected. Thus, the decimated data propose a smoother statics solution. Though the decimated data statics and the original data statics are slightly different in details, they both exhibit the same general trend for the PS statics (the red dashed line). This demonstrates that CCSW has a potential to address converted waves static corrections where geophone interval is wide. Unfortunately, the Priddis data do not contain strong PS events for us to apply and evaluate the calculated statics. Therefore, we analyzed the Hussar data, which contain strong converted waves.

## PS STATIC CORRECTIONS (HUSSAR DATA)

We estimate an S velocity model for the Hussar data in order to calculate receiver static corrections. The procedure of sorting the data from shot gathers into cross correlated CMP gathers is similar to that done for the Priddis data, however the offsets of the reference traces are about 10 m. In this data set, a wide range of wavelengths is observable. Therefore, we use a wavelength-dependent aperture for these data. Figure 12a shows a phase velocity image for a CMP gather whose maximum wavelength is about 150 m. The aperture length is 80 m. At low frequencies (4 Hz to 8 Hz), where the wavelengths are large, it is very hard to pick the phase velocity due to the low resolution of dispersion curves. This is explained by unsuitable aperture length because it is much smaller than the wavelengths at these frequencies. However, at higher frequencies (10 Hz to 15 Hz), where the wavelengths are in the order of 20 m, we can see a better trend of the dispersion curve and therefore the phase velocity is easily detectable. Figure 12b shows the estimated phase velocity for the same CMP gather where the aperture length is 200 m. The phase velocity is obvious on the high resolution images of dispersion curves because, as discussed earlier, the aperture length is close to the maximum wavelength. Figure 12c shows dispersion curves for another CMP gather whose maximum offset is about 70 m. The aperture length is 80 m. Clear images of dispersion curves are noticeable for all frequencies from 4 Hz to 15 Hz because of the suitable length of the aperture. The aperture length (80 m) is close to the maximum wavelength (70 m). We obtain a 2D image of the phase velocity based on an aperture wavelength dependent analysis of the CMP gathers. Figure 13 shows the 2D phase velocity image for the Hussar data. A low phase velocity zone from 2000 m to 2500 m distance is noticeable, which can be inferred to be a channel. Another low phase velocity is observed from 3500 m to 4200 m distance. Two smaller low phase velocity zones can be seen from 800 m to 1200 m and from 1500 m to 1700 m distance. Based on the inverse procedure as explained for the Priddis data, we obtain a 2D image of the S velocity for the Hussar data. Since the maximum wavelength is 90 m, the maximum depth of investigation is assumed to be about 45 m (the half of the maximum wavelength (Xia et al. 1999)). Figure 14 shows the estimated S-wave velocity model for the Hussar data. Two interpreted major channels are seen from 2000 m to 2500 m and from 350 0m to 4200 m distances, which correspond to the two major low phase velocity zones in Figure 13. Two smaller channels are observable from 800 m to 1200 m and from 1500 m to 1700 m distances, which correspond to low phase velocity zones in Figure 13. The S-wave velocity fluctuates with distance. This is expected in the near surface where the weathered layer causes dramatic velocity variations. We calculate static correction from the S-wave velocity model. The black solid line in Figure 15 indicates the static corrections for the Hussar data, which vary from -40 ms to 50 ms. The static corrections in Figure 15 are calculated from the difference between static corrections at any CMP location and the average of the total static corrections. The largest static corrections, which are about 50 ms, are seen from 2000 m to 2500 m distance, corresponding to one of the major channels interpreted in Figure 14. We apply the static correction to the Hussar data to assess the validity of the calculated statics.

Figure 16a shows the stacked data without statics corrections. Flat reflectors are perturbated due to the weathered layer. Figure 16b shows the stacked data after applying the calculated statics. Perturbations are removed significantly. This demonstrates that the

calculated statics are reasonable enough to address static correction for these data. However, there are still some small perturbations. In order to remove the reminding statics, we apply residual statics (Figure 17). We see a clear image of the flat reflectors. The red dashed line in Figure 15 indicates the total statics obtained from the calculated statics and the residual statics added together. Though at the most station locations there is a good match and compatibility between the calculated statics and the total statics, a significant difference is seen from 2000 m to 2500 m distance, where there is an interpreted major channel with a low phase velocity zone. There are two possibilities for this discrepancy. One is the limited bandwidth of the ground roll. The minimum detectable ground roll frequency for this data set is about 4.5 Hz, which confines the depth of investigation to about 45 m. If there had been more low frequency components, we could have investigated deeper layers and consequently used more information in the statics calculation. Another possibility is poor acquisition at the location of the interpreted major channel. This interpreted channel is a very low phase velocity zone, where we should choose a small aperture. When the geophone interval is wide and the aperture is small, we have only few traces in each CMP gather. This causes a low resolution image of dispersion curves because the phase velocity estimation is based on slant stacking methods where fold number is very important for resolution. For instance, in a CMP gather where the maximum wavelength is 30 m, an optimum aperture length should be close to 30 m (40 m for example). When the geophone interval is 10 m and the aperture is 40 m, the fold is four, which results in a low resolution image of dispersion curves (Figure 18). In order to improve the resolution of dispersion curves, we have to increase the aperture beyond its optimum values. This causes the dispersion curves and the estimated phase velocity to be affected by the other velocity structures in the vicinity of the CMP gather. Therefore, at a low velocity zone surrounded by a higher velocity field, we obtain smaller values for statics than if we were able to analyze the low velocity zone without influence from the surrounding higher velocities.

We calculate S-wave refraction statics from the P wave receiver refraction static as a conventional method for comparison with S-wave receiver statics obtained from CCSW. We scale the P-wave receiver statics by 2.5 based on an assumption that $V_p/V_s$ ratio is 2.5 and apply these statics to the data. Figure 19 shows the stacked data after applying the scaled P-wave receiver refraction statics. Comparing Figure 19 with Figure 16b, we observe that the CCSW statics provide better corrections. Figure 20a shows a shot record without receiver static corrections and Figure 20b shows the same record after applying CCSW static corrections. We see better coherence of reflectors after applying the S-wave static correction. Figure 21 shows NMO velocity analysis for a CMP gather before and after application of the calculated S–wave receiver statics. NMO velocity analysis has improved significantly after applying the S-wave receiver statics.

## CONCLUSIONS

We introduce a new approach of the CMP Cross-Correlation of Surface Wave in order to obtain better lateral resolution for near surface S-wave velocity imaging. The idea takes advantages of SASW and MASW methods, is faster than the conventional CCSW (Hayashi and Suzuki, 2004) and is also more robust in the presence of a variable source wavelet and noise.

We define an optimum aperture length for maintaining lateral resolution and dispersion curves simultaneously. According to our results, the aperture length must be close to (one to one and half times) the maximum wavelength. This gives us a better coherency of the fundamental mode and avoids modal interferences.

The detailed static corrections calculated for the dense Priddis data from the S velocity model in this study demonstrate the potential of the method to be utilized in seismic exploration where the receiver interval is not ideal. The decimated data and the original exhibit the same general trend of receiver static corrections. This shows the potential of the method to address converted wave receiver static corrections when the geophone interval is wide.

In order to have a good estimation of the phase velocity where there are wide ranges of wavelengths, a wavelength dependent aperture must be utilized. The general result of the calculated statics of the Hussar data demonstrates the capacity of CCSW to address converted wave receiver static corrections. Application of residual statics improves the image.

Our ability to successfully extract information from converted waves and S-waves is dramatically hampered by our lack of understanding of the near-surface S-wave velocity structure. This is exactly why the surface wave methods should be taken into account. However, if we want to obtain more reliable results from surface waves, we will have to optimize acquisition parameters in areas where there are very low velocity zones. We should also consider the limitations of surface-wave methods such as the modal superposition, which can cause error in the estimation of the phase velocity.

## ACKNOWLEDGEMENTS

The authors wish to express their gratitude to CREWES and its sponsors for their generous support. We express our appreciation to Dr. Robert Herrmann for providing Computer Programs in Seismology and Kevin Hall for his help during the project.

## REFERENCES

Askari, R., Ferguson, R. J., Isaac, H., 2013, Optimum aperture length for improving dispersion curve analysis in CMP Cross- Correlation of Surface Waves: GeoConvention 2013, Calgary, AB.

Askari, R., and Ferguson, R. J., 2012, Estimation Dispersion and the dissipative characteristics of surface waves in the generalized S-transform domain: Geophysics, **77**, 11-20.

Askari, R., Ferguson, R. J. and K. DeMeersman, 2011, Estimation of phase and group velocities for multi-modal ground roll using the 'phase shift' and 'slant stack generalized S transform based' methods: CREWES Research Report, **23**, paper 4.

Cary, P. W., and Eaton, D. W. S., 1993, A simple method for resolving large converted-wave (P-SV) static: Geophysics, **58**, 429-433.

Eaton, D. W. S., Cary, P. W., and Schafer, A. W., 1991, Estimation of P-SV statics using stack-power optimization: The CREWES Research Report: University of Calgary, **3**.

Feng, S., Sugiyama, T. and Yamanaka, H., 2005, Effectiveness of multi-mode surface wave inversion in shallow engineering site investigations: Exploration Geophysics, **36**, 26-33.

Frasier, C., and Winterstein, D., 1990, Analysis of conventional and converted mode reflections at Putah sink, California using three-component data: Geophysics, **55**, 646-659.

Hayashi, K., and H. Suzuki, 2004, CMP cross-correlation analysis of multi-channel surface-wave data: Exploration Geophysics, 35, 7–13.

Li, Y., Ma, Z., Sun, P., and Yang, H, 2012, Converted-wave static correction method for thick weathering area: Chinese Journal of Geophysics, **55**, 76-83.

Ikeda, T., Tsuji, T., and Matsuoka, T., 2013, Window-controlled CMP cross-correlation analysis for surface waves in laterally heterogeneous media: Geophysics, in revision.

Ivanov, J., C. B. Park, R. Miller, and J. Xia, 2000, Mapping Poisson's ratio of unconsolidated materials from a joint analysis of surface-wave and refraction events: Proceedings of the Symposium on the Application of Geophysics to Engineering and Environmental Problems (SAGEEP 2000), Arlington, VA, February 20–24, 11–20.

Nazarian, S., K. H. Stokoe, and W. R. Hudson, 1983, Use of spectral analysis of surface waves method for determination of moduli and thickness of pavement system: Transportation Research Record, **930**, 38–45.

Park, C. B., R. D. Miller, and J. Xia, 1998, Imaging dispersion curves of surface waves on multi-channel record: 68th Annual International Meeting, SEG, Expanded Abstracts, 1377–1380.

Park, C. B., R. D. Miller, and J. Xia, 1999a, Multichannel analysis of surface waves: Geophysics, **64**, 800–808.

Park, C. B., R. D. Miller, and J. Xia, 1999b, Multimodal analysis of high frequency surface waves: Proceedings of the Symposium on the Application of Geophysics to Engineering and Environmental Problems (SAGEEP), 115–121.

Schwab, F. A., and L. Knopoff, 1972, Fast surface wave and free mode computations, in B. A. Bolt, ed., Methods in computational physics: Academic Press, 87–180.

Strobbia, C., Laake A., Vermeer P., and Glushchenko A., 2011, Surface-waves: use them then lose them. Surface-wave analysis, inversion and attenuation in land reflection seismic surveying, Near-surface Geophysics, **9**, 1-12.

Tatham, R. H., and McCormack, M. D., 1991, Multicomponent seismology in petroleum exploration: Society of Exploration Geophysicists.

Xia, J., R. D. Miller, and C. B. Park, 1999, Estimation of near-surface shear-wave velocity by inversion of Rayleigh waves: Geophysics, **64**, 691–700.

Zeidouni, M., 2011, Analytical and inverse models for leakage $CO_2$ storage: Ph.D. dissertation, University of Calgary.

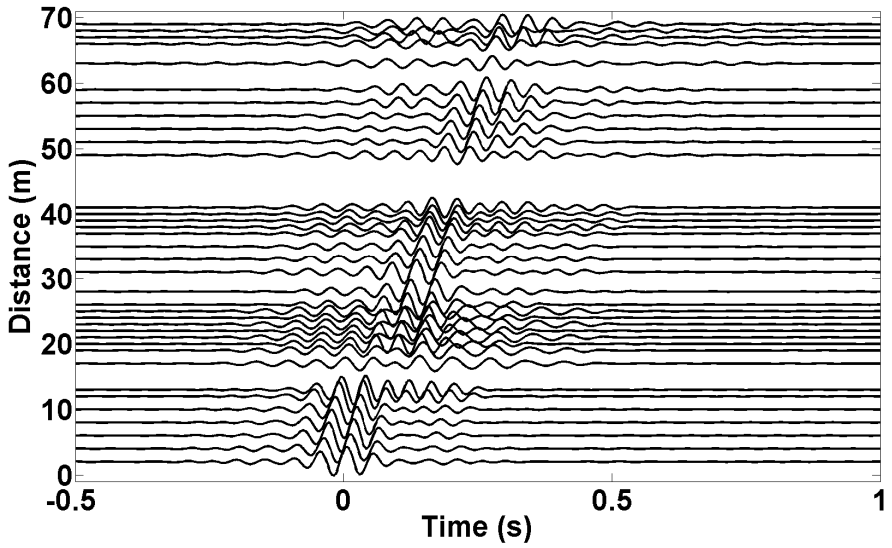


Fig. 1. Traces in a bin.

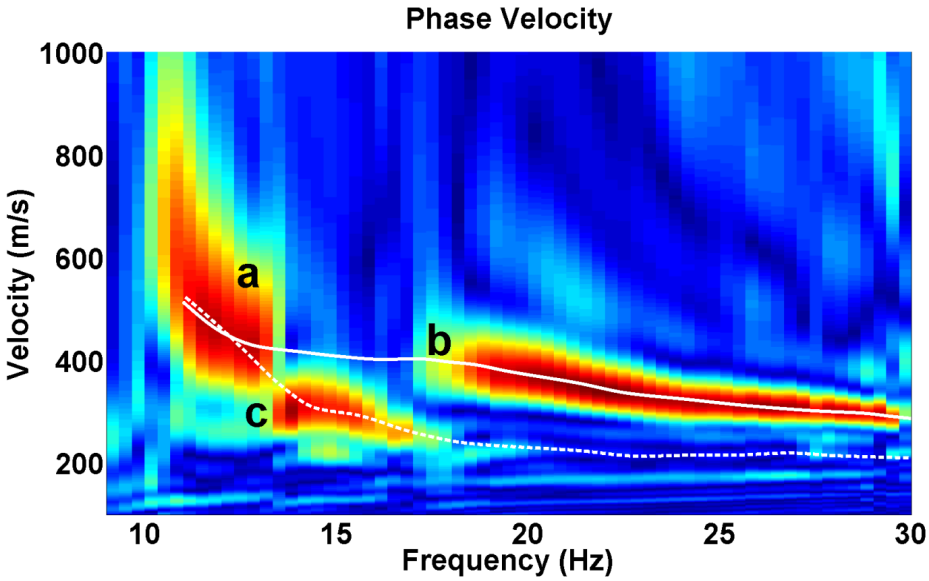


Fig. 2. The phase velocity for the record in Figure 1.

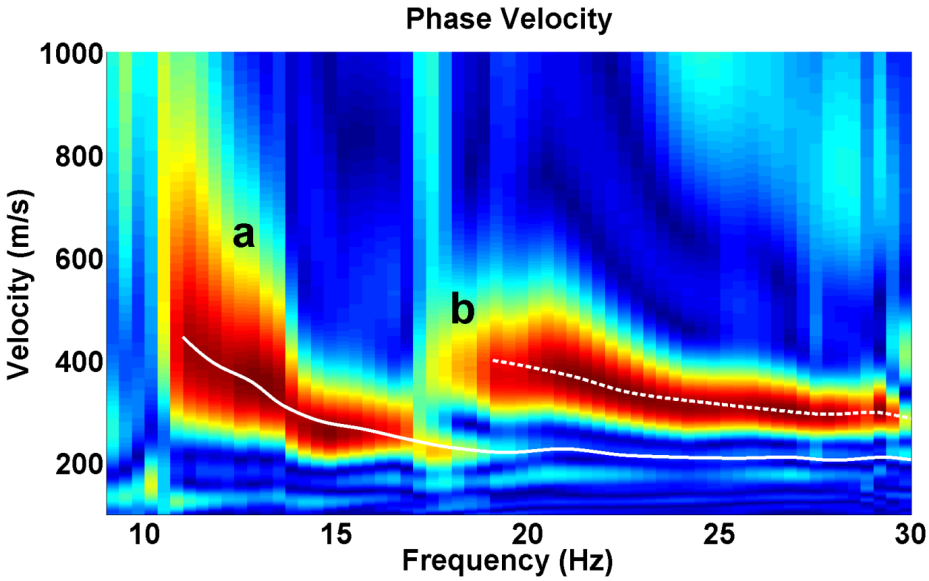


Fig. 3. The phase velocity for the record in Figure 1 with aperture length 45 m. The solid line is the fundamental mode and the dashed line is the first higher mode.

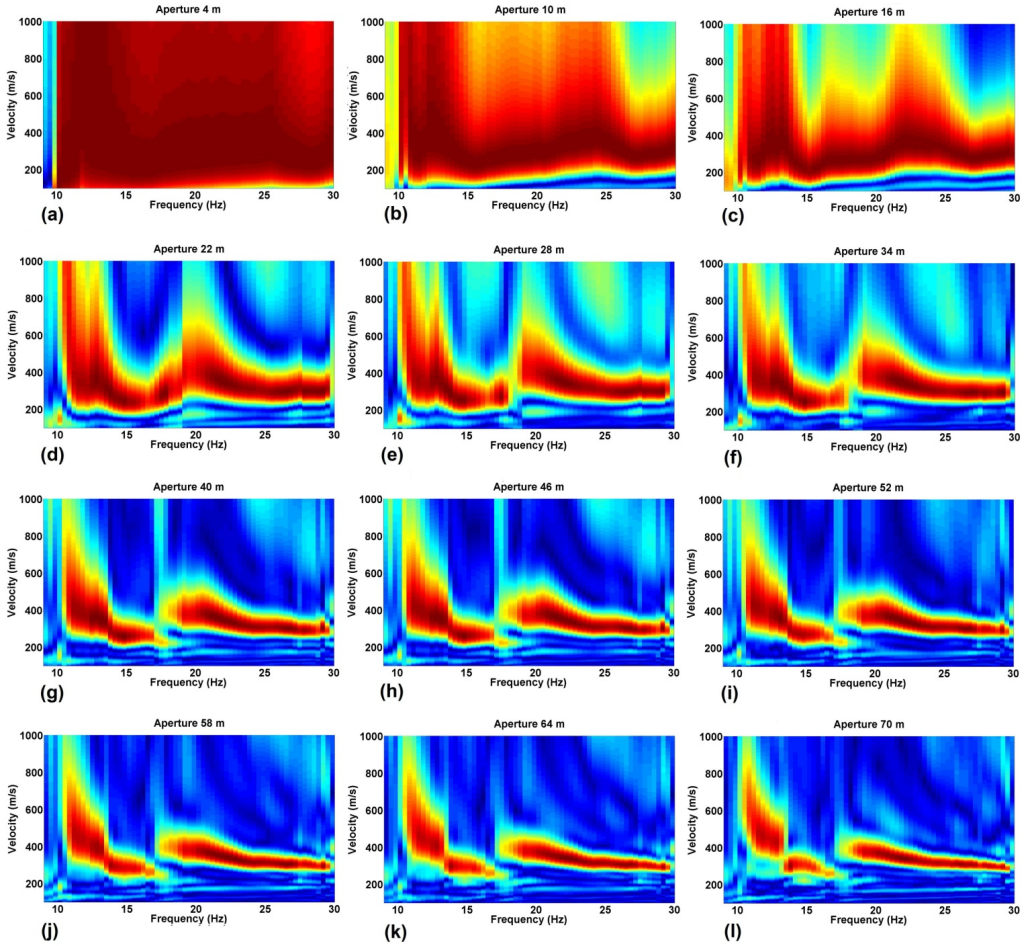


Fig. 4: Evolution of dispersion curves. The aperture length increases from 4 m (a) to 70 m (l) in steps of 6 m.

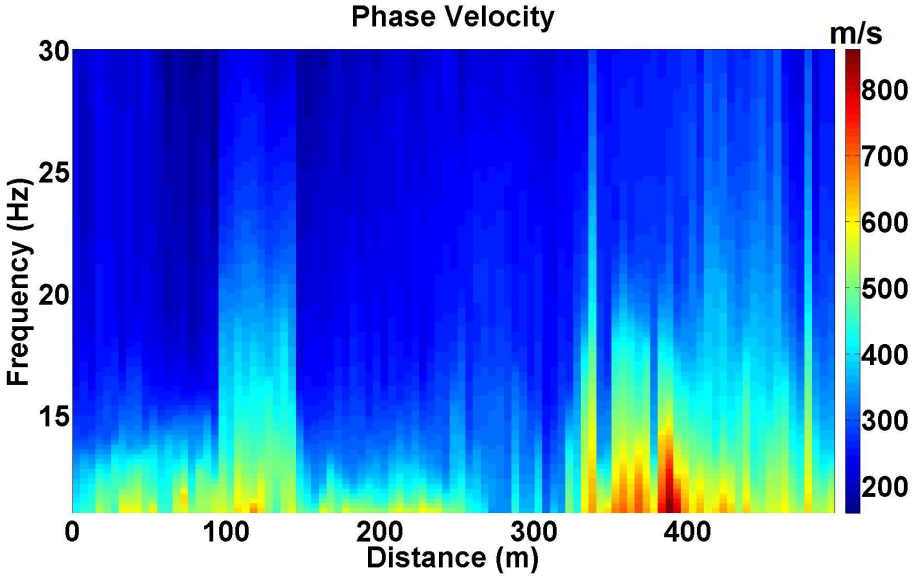


Fig. 5. The estimated phase velocity for the Priddis data.

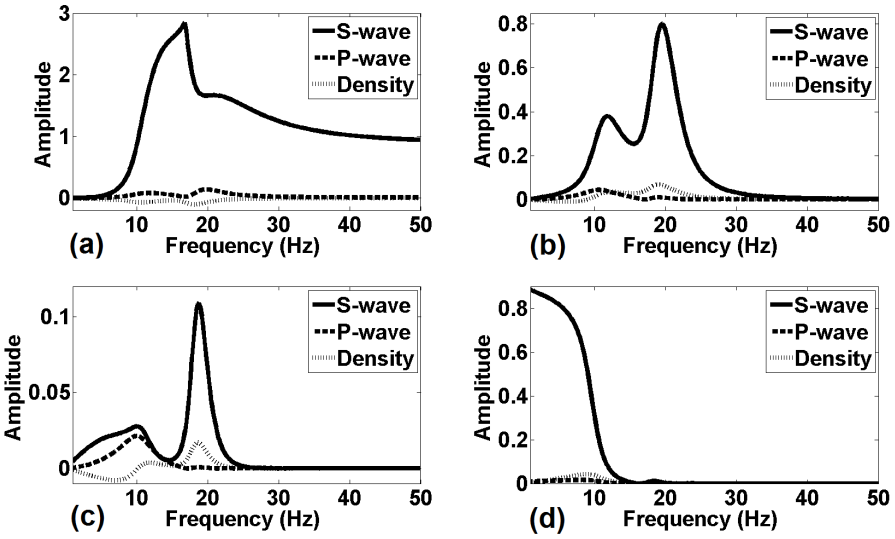


Fig. 6. Phase velocity derivatives with respect to S, P velocities and density respectively for (a) the first layer, (b) the second layer, (c) the third layer and (d) the forth layer.

| S Velocity | P velocity | Density |
|---|---|---|
| 200 | 500 | 2000 |
| 400 | 1000 | 2000 |
| 600 | 1500 | 2000 |
| 900 | 2250 | 2000 |

Table 1. The geological model used for the calculation of the derivatives in Figure 6. The thickness of each layer is 4 m.

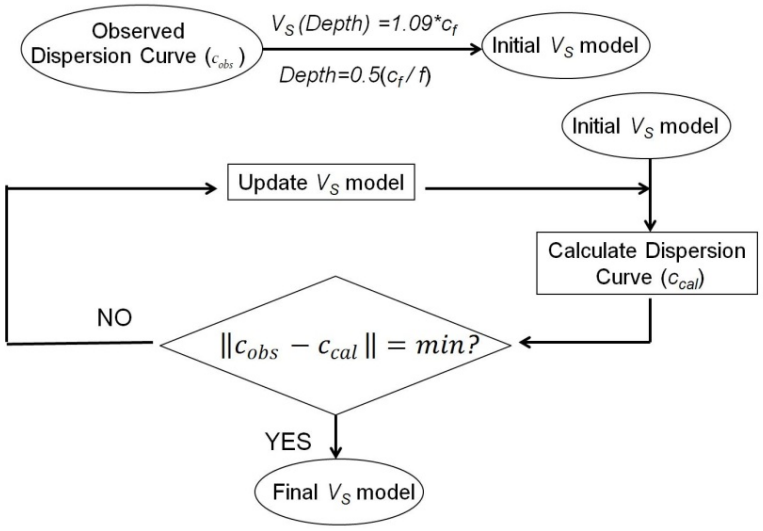


Fig. 7. The inverse procedure used for the estimation of shear wave velocity from the phase velocity. An initial S-wave velocity model is calculated. Then, we calculate the theoretical phase velocity model and compare it to the observed phase velocity obtained from field data. If the norm of the difference of the observed and calculated phase velocities is small enough, we terminate the process; otherwise, we update the S-velocity model using an inverse method (Conjugate Gradient for example). After some iterations, we will obtain the final S-wave velocity model.

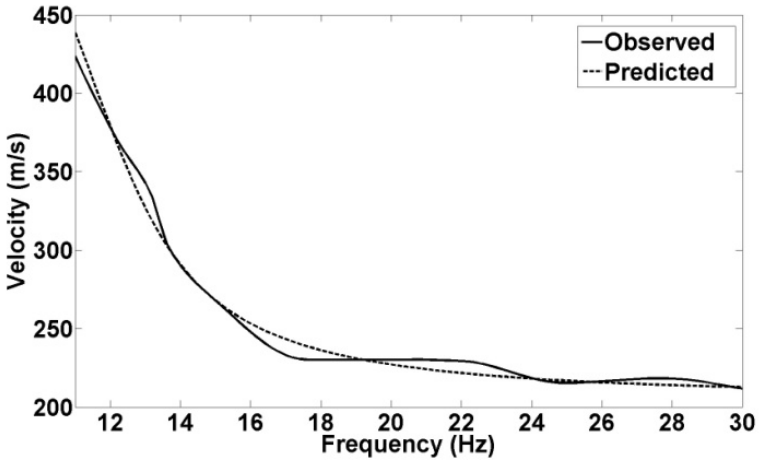


Fig. 8. The predicted phase velocity (the dashed line) versus the observed phase velocity in Figure 3 (the solid line).

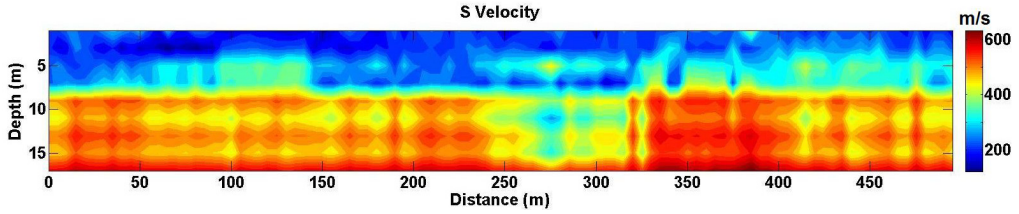


Fig. 9. The S-wave velocity model for the Priddis data obtained from the phase velocity in Figure 5.

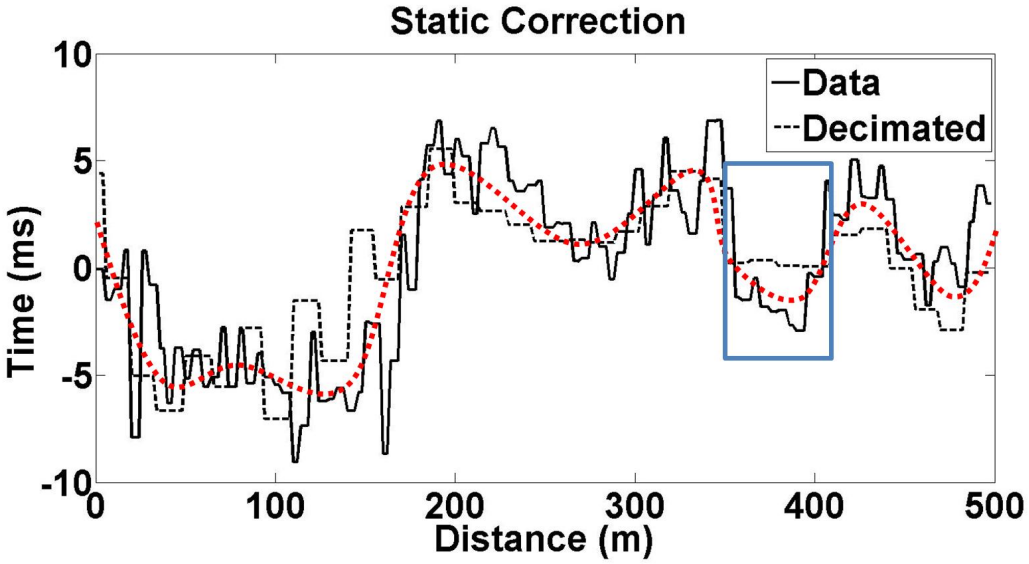


Fig. 10. Static corrections for the Priddis data (the solid line) and the decimated data (the black dashed line).

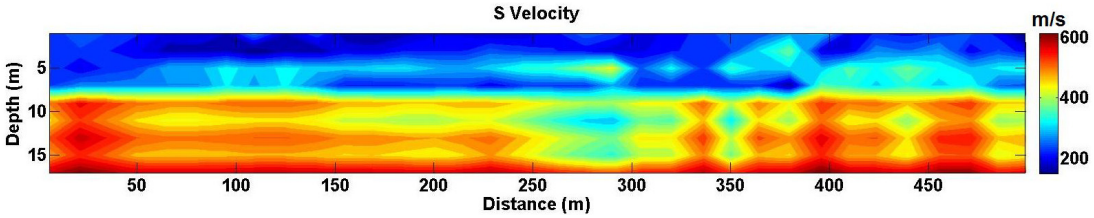


Fig. 11. The S-wave velocity model for the decimated data.

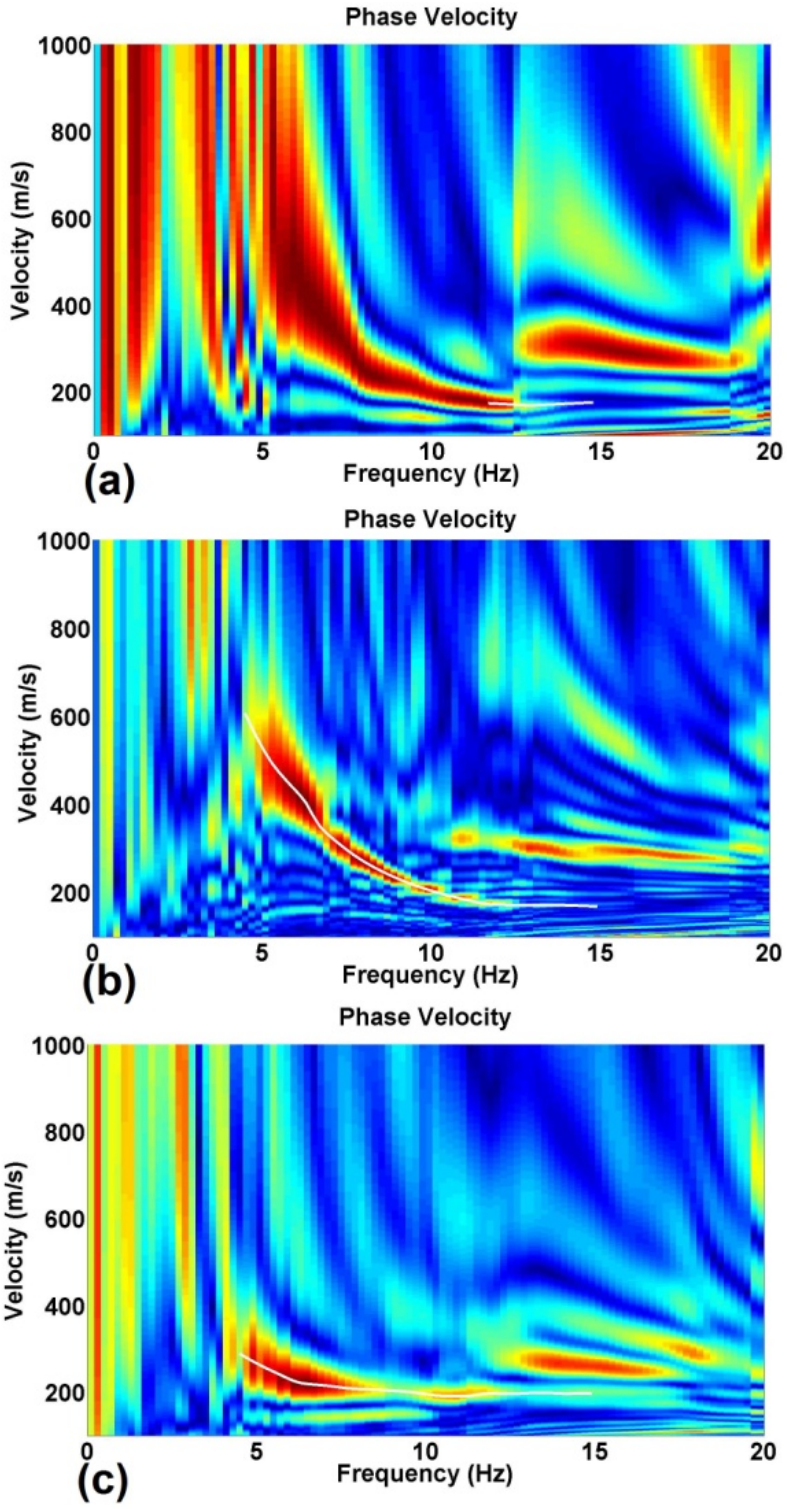


Fig. 12. (a) Dispersion curve analysis for a CMP gather when the aperture length is 80 m. (b) Dispersion curve for the same CMP gather when the aperture length is 200 m, and (c) dispersion curve analysis for a CMP gather whose maximum wavelength is 70 m and the aperture length is 80 m.

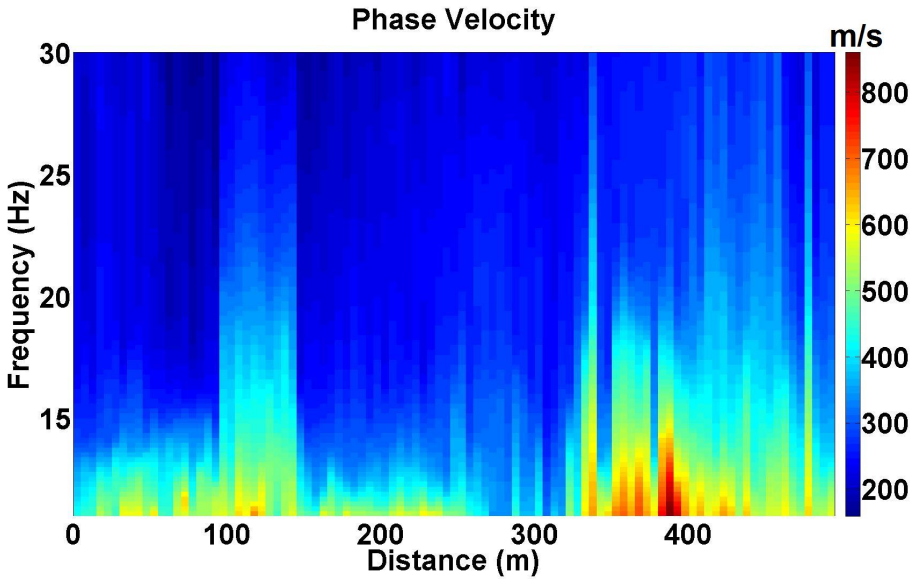


Figure 13: The estimated phase velocity for the Hussar data.

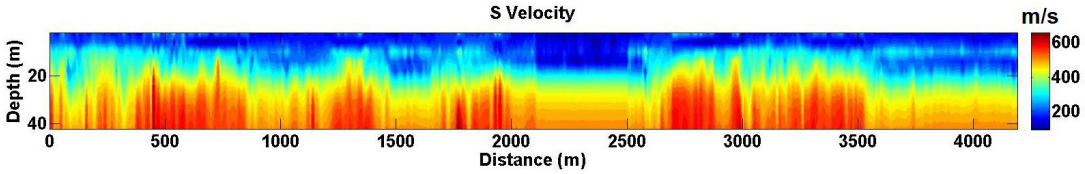


Fig. 14. The S velocity model for the Hussar data obtained from the phase velocity in Figure 13.

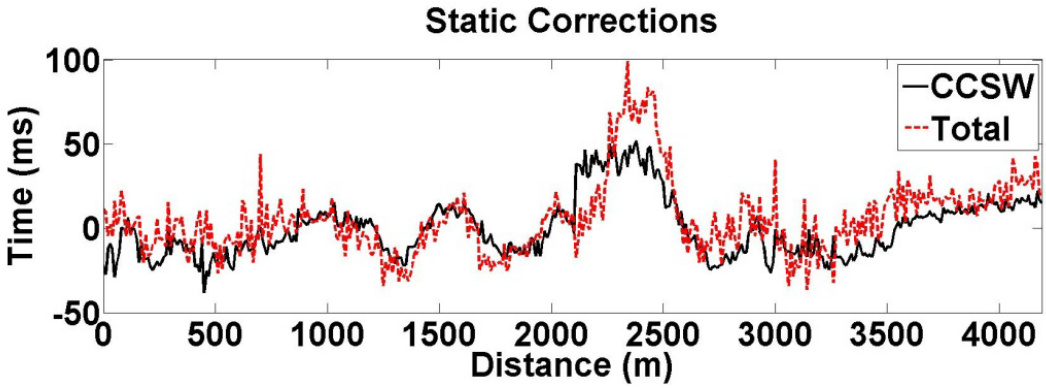


Fig. 15. Static corrections for the Hussar data.

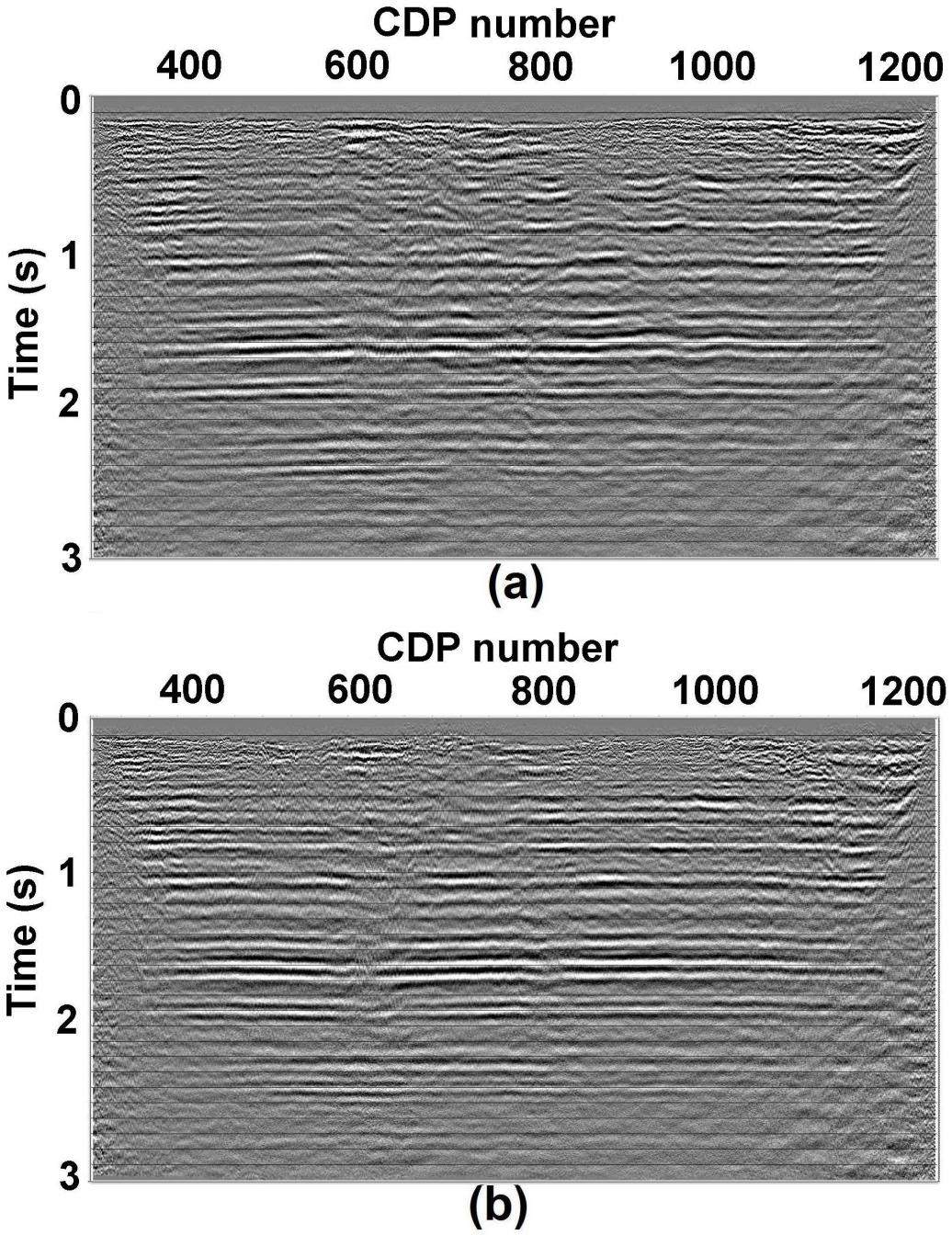


Fig. 16. (a) Stacked Hussar data before static correction, (b) the stacked data after applying the calculated S-wave receiver static.

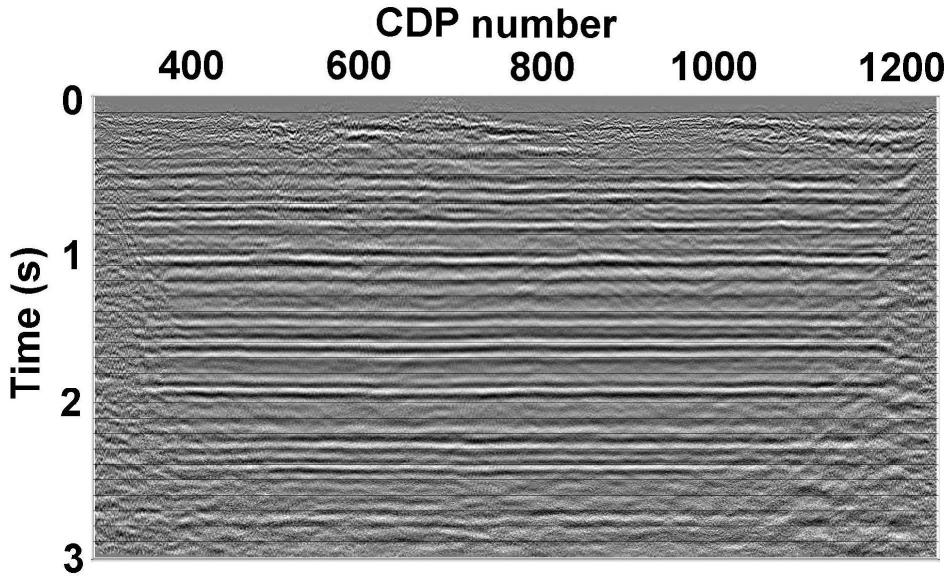


Fig. 17. The stacked data after applying residual statics.

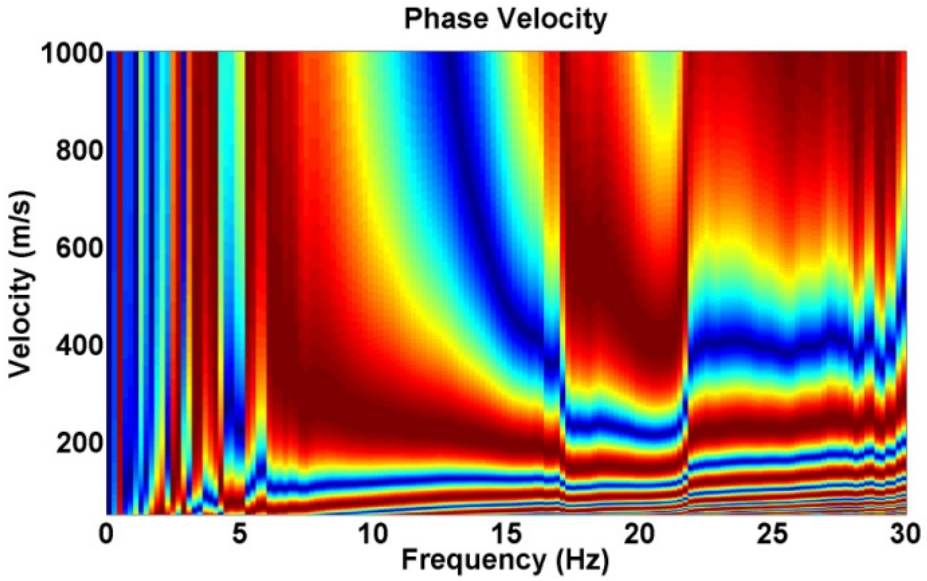


Fig. 18. The phase velocity estimation for a CMP gather whose fold number is four. We see vague trends of dispersion curve which are due to modal imposition.

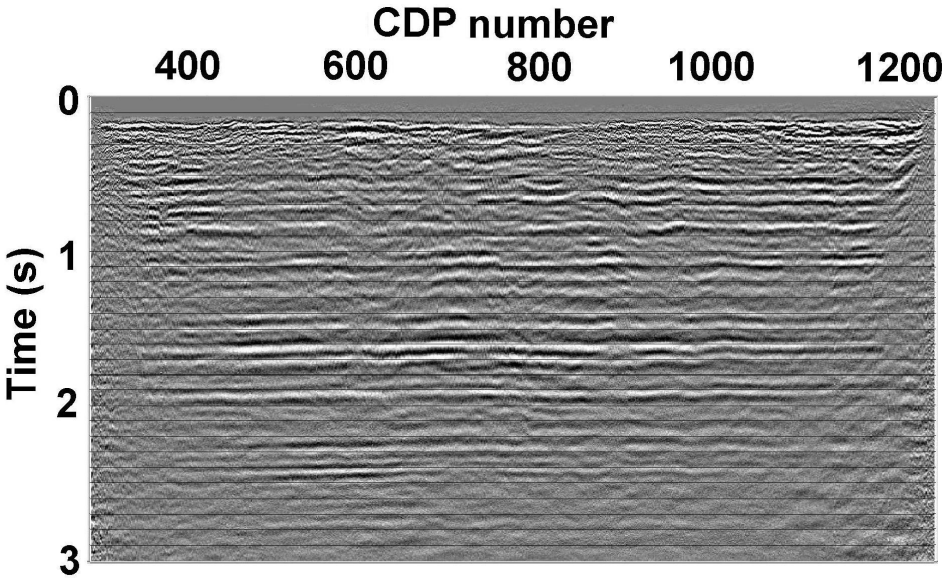


Fig.19. Stacked data with the P-wave receiver refraction statics scaled by 2.5 applied to the data as S-wave receiver statics.

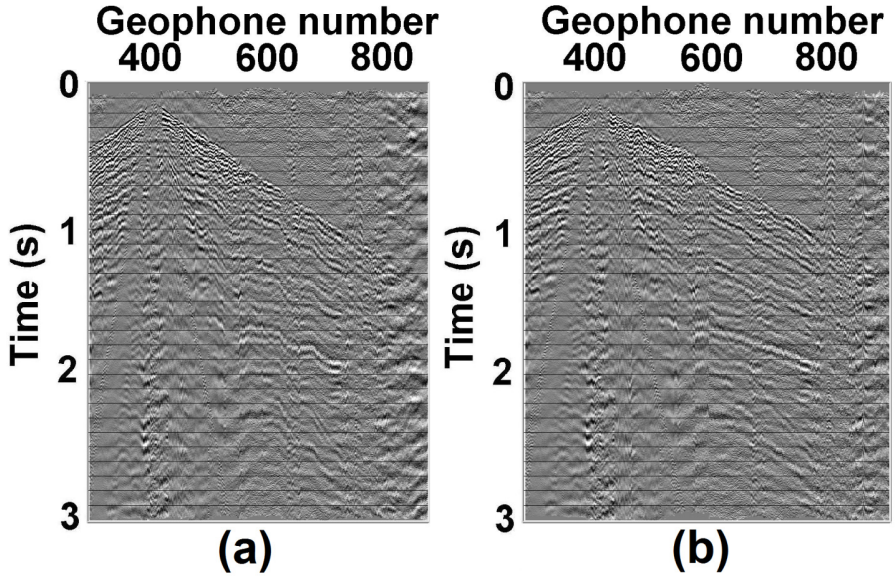


Fig. 20. A shot record, (a) before without static corrections, and (b) after applying static corrections.

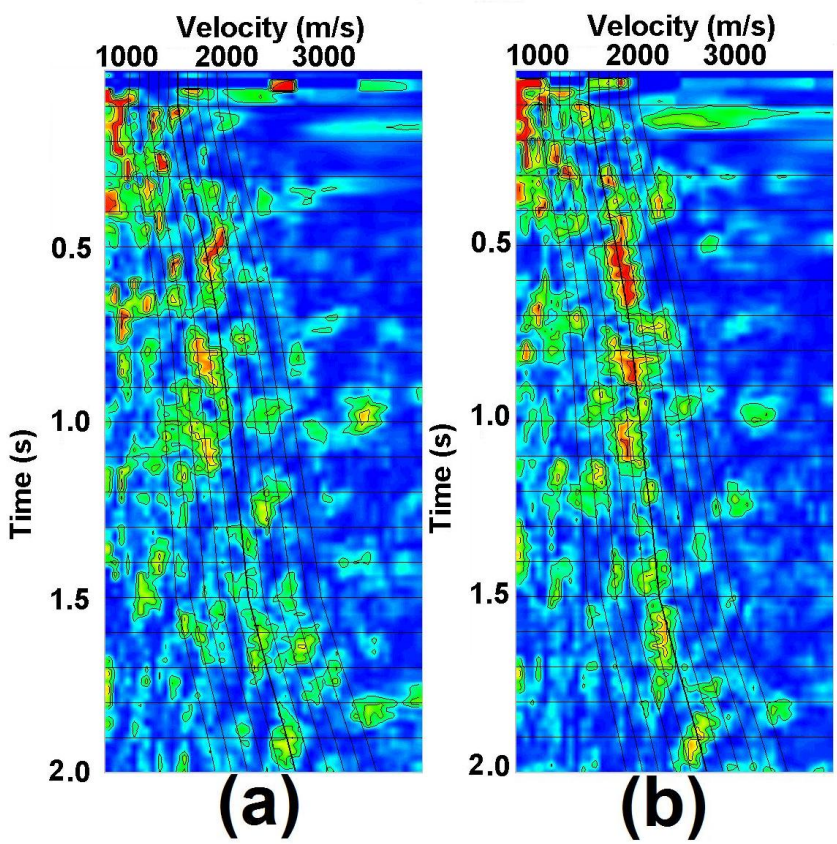


Fig. 21. NMO velocity analysis. (a) before static correction and (b) after applying the calculated statics.